# Influence of low CO concentration on catalysed carbon deposition on 20Cr25Ni steel in $CO_2$ environments containing ethene

Ding, Rengen; Taylor, Mary; Evans, Hugh; Mowforth, Clive; Smith, Neal; Chiu, Yu-Lung; Connolly, Brian

*DOI:*
10.1016/j.corsci.2018.08.015
10.1016/j.corsci.2018.08.015



*Document Version*
Peer reviewed version

*Citation for published version (Harvard):*
Ding, R, Taylor, M, Evans, H, Mowforth, C, Smith, N, Chiu, Y-L & Connolly, B 2018, 'Influence of low CO concentration on catalysed carbon deposition on 20Cr25Ni steel in $CO_2$ environments containing ethene', *Corrosion Science*, vol. 143, pp. 56-64. https://doi.org/10.1016/j.corsci.2018.08.015, https://doi.org/10.1016/j.corsci.2018.08.015

# Influence of low CO concentration on catalysed carbon deposition on 20Cr25Ni steel in $CO_2$ environments containing ethene.

R. Ding[1], M.P. Taylor[1], H.E. Evans[1], C.W. Mowforth[2], N. Smith, Y.L. Chiu[1] and B.J. Connolly[3]

1) School of Metallurgy and Materials, University of Birmingham, Birmingham, B15 2TT, UK.
2) EDF Energy, Barnwood, Gloucester, GL4 3RS, UK.

3) Formerly at the University of Birmingham, now at University of Manchester, UK.

## Abstract

Carbon deposition on 20Cr25Ni steel at 700°C has been investigated in $CO_2$-based gases containing 0.7 vol%, 1.0 vol% and 1.4 vol% CO, each with ~1000vpm $C_2H_4$, at 700°C. Filamentary carbon deposits were formed at the two lowest CO contents but not at 1.4 vol% CO. TEM analyses have shown that the different CO levels change the propensity for deposition by altering the ratio of Ni:Fe in the nanometre sized catalytic particles produced during oxidation.

## 1. Introduction

Austenitic stainless steels are a very useful class of alloys combining good oxidation resistance with potential for high creep strength. They are employed widely in the petrochemical industry and the variant 20Cr-25Ni (wt.%) is used in the UK as fuel cladding in the Advanced Gas-cooled (nuclear) Reactors (AGRs). However, the formation of carbon deposits commonly occurs on the alloys at elevated temperatures in gaseous carbon-bearing environments having carbon activities, $a_c$ >1. Such deposits can have significant detrimental effects, e.g. by reducing heat-transfer efficiency or may be associated with excessive carburization of the alloy [1-4] and consequent structural impairment or, in extreme cases, metal dusting [5-7].

Carbon deposition on a Si-free model 20Cr25Ni austenitic steel from a $CO_2$-based gas containing ethene is catalysed by Ni-rich metal particles [8], usually some tens of nanometres in size. In gaseous environments having oxygen potentials sufficient to oxidise Fe and Cr, for example, such Ni-rich particles form within a porous oxide layer in the early stages of

oxidation [8]. The catalytic activity of Ni in these alloys is unsurprising in view of earlier work [9] that showed that carbon deposits could readily form on pure Ni. Gas access to these particles is necessary for the catalysed deposition process to take place and the presence of protective surface oxide layers (e.g. chromia or silica) provides an effective method of preventing this [1,8,10-14]. This can be achieved either through a pre-oxidation stage [9] or by introducing short-circuit diffusion paths (dislocations, small grains) for Cr or Si within the surface regions of the alloy [10-12].

The aim of the present work is to examine further the nature of the catalytic particles formed during the early stages of oxidation of the 20Cr25Ni austenitic steel. Previous work [8], using TEM supplemented by EDS analysis, found that in 4-hour exposures in $CO_2$, 1%CO, 1000vppm $C_2H_4$ at 550$^o$C, the catalytic particles were essentially pure Ni and 10-20 nm in size. The current work uses a similar approach to determining particle compositions but employs FIB sectioning to increase the number of particles examined. The work also uses the higher test temperature of 700$^o$C to increase reaction rates and particle numbers produced in the early stages of oxidation. In addition, the effect of changes to the CO content of the depositing gas on particle compositions, their size and the propensity to form deposits is examined.

## 2. Experimental procedure

The alloy used was a stabilised Si-free austenitic steel of composition (wt%) 19.0Cr, 26.5Ni, 53.2Fe, 0.6Nb and 0.67Mn, the carbon content of the steel was 0.015 wt.%. The composition was determined by wet analysis and confirmed using EDS analysis for the metallic elements, and the alloy was available as cold-worked strip of ~ 0.4 mm in thickness. The cold-rolled alloy strip was sectioned into rectangular samples of approximately 10 mm × 20 mm. The cold-rolled surfaces were then ground and polished so as to remove a minimum of 50 μm of material from both surfaces, thus ensuring that no defects in the surfaces caused by the cold-rolling process remained. To remove residual stresses and create a microstructure consisting of equiaxed emergent surface grains of 3 to 10 μm diameter, the specimens were heat treated at 930°C for 30 min in a non-oxidising atmosphere of 5% hydrogen in argon. The final stage in the preparation process involved electro-polishing in 10% perchloric acid in acetic acid, followed by ultrasonic cleaning in ethanol.

The samples were placed on alumina boats and positioned inside a purpose built rig. Details of this rig are available in ref. 15. The rig was purged with a non-oxidising (5%$H_2$/Ar) gas and brought up to the exposure temperature of 700°C at a ramp rate of 20°C $min^{-1}$. The gas was changed to the test gas, details given below, for four hours. After exposure the gas was changed back to the 5% hydrogen in argon gas and the furnaces cooled overnight. The gas flow throughout was maintained at approximately 0.3 $l.min^{-1}$. These specimens were subsequently examined and not exposed further to the depositing environment. This procedure ensured that the deposit structure developed during the oxidation stage was preserved. As will be shown, the spinel oxide formed during this stage was $(Fe,Cr)_3O_4$, containing no Ni, and so Ni-rich metallic particles could not be produced by spinel reduction as has been found elsewhere [15].

Gases with different carbon monoxide concentrations were employed in the testing conducted here, supplied as pre-mixed bottles, with nominal compositions of 0.7, 1.0 or 1.4% CO / 1000vppm ethene / bal. $CO_2$. All deposition tests were conducted at 1 atmosphere total pressure at a temperature of 700°C for 4 hours. The gases were exhausted through an extraction system producing a thermodynamically open system. The oxygen partial pressure, $P_{O2}$, of these gases is dominated by the CO/$CO_2$ equilibrium:

$$2CO + O_2 \rightarrow 2CO_2 \qquad (A)$$

according to:

$$P_{O_2} = \frac{p}{p^*} = \frac{P_{CO_2}^2}{P_{CO}^2} \exp\left(\frac{\Delta G_A^o}{RT}\right) \qquad (1)$$

where p is the partial pressure of oxygen in the gas having a total pressure of 1 atmosphere, p* is the oxygen standard state of 1 atmosphere, $P_{O2}$ is thus the fractional partial pressure and is dimensionless. $P_{CO2}$ and $P_{CO}$ are the partial pressures of $CO_2$ and CO respectively, $\Delta G°_A$ is the standard free energy change for reaction (A), R is the ideal gas constant (8.314 $J.K^{-1}.mol^{-1}$) and T is temperature in K. Estimated values of $P_{O2}$ at 700°C are $1.1x10^{-17}$, $5.5x10^{-18}$ and $2.8x10^{-18}$ for the 0.7% CO, 1.0% CO and 1.4% CO gases, respectively. The calculations use the standard free energy change, $\Delta G_A^o$, of -396000 J/mole $O_2$ [17]. Fe and Cr in the alloy oxidise in the $CO_2$/1%CO environment [8, 16] but Ni will not, even at unit activity of the metal. Calculations for $P_{O2}$ for the gases at 700°C are shown above whereas the calculated $P_{O2}$ for formation of NiO from pure Ni at 700°C is $7.8x10^{-17}$. The calculations intentionally take unit activity for Ni since early investigations showed essentially pure Ni particles

resulted from the initial stages of oxidation of the alloy and these particles act as catalysts for carbon deposition at 550°C [8]. It will be shown later in this work, at 700°C, that the particles formed are highly Ni-rich.

The carbon activity, $a_c$, of the gases is dominated by the oxidation of ethene by both $CO_2$ and CO and various possible overall reactions can be identified [8]:

$$C_2H_4 + 2CO_2 \rightarrow 2C + 2CO + 2H_2O \quad (B)$$

$$C_2H_4 + 2CO \rightarrow 4C + 2H_2O \quad (C)$$

$$C_2H_4 + CO_2 \rightarrow 3C + 2H_2O \quad (D)$$

$$2CO \rightarrow CO_2 + C \quad (E)$$

The carbon activities for the reactions have been previously calculated at 550°C as **$9.2 \times 10^6$, $2.1 \times 10^2$ and $7.5 \times 10^3$** for reactions B to D respectively, using ThermoCalc [8]. A similar assessment at 700°C produced activities of **$2.1 \times 10^6$, $2.5 \times 10^2$ and $5.1 \times 10^3$**. The actual reaction path is unclear but values of $a_c >> 1$ are generated by this gas mixture and carbon deposits were formed in the present tests. Carbon activities generated through Reaction (E) are negligibly small at $a_c \sim 10^{-4}$; calculations from Thermocalc give values of $1.8 \times 10^{-4}$ for 0.7% CO, $2.7 \times 10^{-4}$ for 1% CO and $4.2 \times 10^{-4}$ for 1.4% CO at 700°C. This reaction does not contribute significantly to carbon deposition. Thus, changes in the concentration of CO in the deposition gases used here will not produce a significant difference in the carbon activity of the three gases.

A dual beam FEI Quanta 3D system consisting of a focussed gallium ion beam (FIB) and conventional field-emission scanning electron (FEGSEM) column, also equipped with an Oxford Instrument Energy Dispersive Spectrometer (EDS), was used to observe the sample surface and for the preparation of TEM foils. Some typical features of the sample surface were cross-sectioned, extracted and thinned by FIB. The initial stages of foil preparation used a 30 kV ion beam with the probe current reduced successively throughout the procedure to a final polishing/cleaning stage performed at 5 kV. These foils were examined in an FEI Tecnai F20 (scanning) transmission electron microscope (STEM) equipped with an Oxford Instrument X-max SDD detector operating at 200 kV.

Particular care was taken when determining the composition of particles entrapped within the oxide layer to negate signal contamination from the surrounding oxide. To undertake this it

was necessary to subtract the contribution from the surrounding oxide from each of the spectra obtained for the particles. To achieve this, the Cr peak was chosen as it can be assumed that any Cr present would have been converted to the oxide and would be absent from the particles. The Cr peak from the EDS spectrum was normalised for both the particle and the oxide signal. Subtraction of the oxide contribution from the combined spectrum then produced the calculated composition of the particle at that site. No such compensation was required for the metallic particles within the carbon deposit.

## 3. Results and discussion

The surfaces of the specimens after the deposition runs were examined using the SEM and typical images are shown in Figure 1. EDS results confirmed that carbon deposits had formed only in the 0.7% and 1.0% CO gases and not in the 1.4% CO gas. Filaments of carbon are shown by the arrows in Figure 1 and these usually had a bright contrast metallic particle at their tip with typical diameter $\leq$ 50 nm. This morphology is broadly the same as found previously [8] in the 1% CO gas for exposures at 550$^{o}$C. Examination of Figure 1 suggests that there are two size ranges of particles present: those of around 50 nm in size that appear to act as catalysts to the deposition process and larger particles, ~500 nm, that do not. Both types of particles appear to be Ni-rich but a more robust evaluation of their composition requires TEM/EDS analysis, as detailed below. Within the context of the present paper, particular emphasis is given to the smaller size range of particles because of their relevance to the deposition process.

TEM cross-sections were prepared from the alloy exposed to each of the three CO gas compositions using FIB milling. Figure 2 shows a montage of STEM images of three exposed samples for each of the gas compositions. These images show details of the alloy with grain boundaries, twins and some sub-surface dark contrast features at grain boundaries underlying the surface oxide. These are voids, possibly Kirkendall in origin, which were enlarged during the milling process as a result of differential sputtering rates. The outer surface of the specimen consists of a continuous oxide of differing thickness. Some regions are thin with an approximate thickness of 100nm and others are up to 500nm thick and more complex, as indicated by the contrast differences within the oxides. These two distinct oxide regions were present at all gas compositions. Carbon deposits were evident on the surface of the samples tested at 0.7 and 1.0% CO as shown as dark contrast (arrowed) in Figure 2 (a and

b); no carbon deposits were found in the sample tested at 1.4% CO (Figure 2c), consistent with the earlier SEM examination (Figure 1). It is interesting that C deposits formed at central grain regions and not at grain boundaries (Figures 1 and 2). This is consistent with previous observations at 550$^{o}$C [8], and arises because the grain boundary is a fast diffusion path for Cr. Chromia then forms rapidly above these emergent grain boundary regions and prevents gas access to any metallic catalytic particles.

Higher magnification examination of the spinel oxide above the central region of a grain is shown in Figure 3 along with electron diffraction patterns taken from the alloy, oxide, particles and the oxide / alloy interface. The oxide was identified as the FCC spinel $(Cr,Fe)_3O_4$ phase with a lattice parameter a=0.84 nm. The alloy and particles within the oxide both have the same FCC structure and orientation indicating that the particles retain some level of connectivity with the substrate until final separation occurs. This demonstrates clearly the proposed method of formation of the particles in that they are formed as a result of the inward growth of the spinel at a rate which isolates and concentrates the un-oxidised Ni component of the alloy. Patterns taken from the interface, Figure 3c, contain components from the alloy and the oxide. EDS analysis of the oxides formed in each gas shows similarity in composition although the confidence in the oxygen concentration is not as good using this technique, Table 1, however, the Cr to Fe ratio in each case is similar. The oxide thickness measurements taken from the three samples were as follows: 249±140nm for 0.7% CO, 262±93nm for 1.0% CO and 290±107nm for 1.4% CO gas mixtures show a slight but not significant increase in the mean values for the regions examined but this is also within statistical scatter of the data, it should be noted that these measurements are from a limited sample range.

EDS was used to analyse compositions of the small particles (tens of nanometres) in the C deposit and within the oxide layer. Figures 4 and 5 illustrate EDS maps for the C deposit and oxide layers for the specimens exposed to the 0.7 and 1.0% CO gases, respectively, and, in Figure 6, for only the oxide layer for the 1.4% CO sample since deposits did not form in this gas. The maps show the particles in the C deposits to be rich in Ni and Fe but containing neither Cr nor O (Figures 4 and 5). The surface oxide layer is predominantly Cr and Fe rich. The particles within the oxide layers are also rich in Ni and Fe. In addition, there are large (~1 μm) particles sitting proud of the surface on top of the oxide (Figure 2) and these again are Ni- and Fe-rich, as shown in Figure 6, with no evidence of their having been oxidised. The results of an EDS linescan across the oxide and grain boundaries in the sample exposed

to the 1.4% CO gas are shown in Figure 7. It demonstrates that a ~100 nm wide Cr depletion region had formed underneath the surface oxide and that some Cr depletion also existed at alloy grain boundaries. This figure also shows that the surface oxide is composed of Cr and O with negligible quantities of Fe or Ni, i.e. $Cr_2O_3$ forms above regions of emerging grain boundaries and grows laterally across the surface.

To understand the influence of CO concentration on C deposition, the number and composition of the Ni-rich particles formed in the early stages of oxidation were investigated. The sizes of the (small size-range) particles within the oxide layer were measured from the STEM images and histograms are given in Figure 8 for the 0.7% and 1.4% CO gas variants. The distributions obviously overlap considerably but the mean of the diameters of the precipitates formed under the 0.7% CO containing gas (39 nm) were greater than those formed under the 1.4% CO containing gas (34 nm). A summary of the findings is presented in Table 2 which gives the mean and standard deviation values for particle diameters. Although the difference in the means is relatively small, the large number of particles measured (>350, see Figure 8) per test condition, produces a t-statistic of ~9, indicating that the difference in the means is highly significant. It may well be that the fraction of smaller particles present in the size distribution developed in the 0.7% CO gas had acted as catalysts and had entered the carbon deposit. Unfortunately, this could not be demonstrated with confidence because of the relatively limited numbers of particles available for measurement within the deposit compared with those within the oxide layer. Table 2 also gives the number densities of the small metallic particles formed within the oxide in the two gases. Broadly similar values were obtained although slightly fewer particles were present after exposure to the 0.7% CO environment consistent with the hypothesis that some (~6% of the total) had entered the C deposit.

As mentioned in the experimental procedure, a subtraction technique was used to determine the composition of the Ni-rich particles within the oxide. The values obtained are given in Table 3 from which it can be seen that there is no systematic variation in the Ni/Fe ratios with the CO content of the gas. The Ni content of the particles averages at around 71 at.% over the range of CO contents. An additional study was undertaken of the particles within the C deposits because these had, by definition, been involved in the deposition process. The compositional results are given in Table 4 but only for the two lowest CO concentrations since no significant C deposits had formed on the sample exposed to the gas containing 1.4% CO. The results of Table 4 show that the average Ni content of the particles within the

deposit for the 0.7% CO gas was 88.8 at.% and for the 1.0% CO gas, 79.6 at.%. They exceeded the average of the measurements made within the oxide for both gases (Table 3).

A systematic study of the propensity for particles of Ni-Fe powders of various compositions to catalyse C deposition has been undertaken by Park and Baker [18]. Their results are illustrated in Figure 9 and show how solid carbon is formed at Ni concentrations greater than approximately 75 at.%. This carbon appears to arise from the dissociation of ethene, as in the present work, because the decrease in the concentration of this compound mirrors the increase in the formation of solid carbon. The following discussion proceeds on the basis that the mechanism of catalysed deposition on the Ni-Fe surface in current tests is the same as in the environment of Park and Baker so that their observed trends of C deposition with Ni content can be applied directly.

The average Ni content (~71 at.%) of the particles within the oxide layer (Table 3) is illustrated as the solid vertical line in Figure 9 and is independent of the CO levels. At this Ni content, the particles would not be expected to catalyse C deposition, on the basis of Park and Baker's work. Indeed, these particles in the present study have not done so because they remain within the oxide layer, unassociated with filamentary carbon. However, the average Ni contents of the particles within the deposit for the 0.7% CO was 88.8 at.% and for the 1.0 CO, 79.6 at. % (Table 4). These values are shown in Figure 9 as the dashed lines and these refer to particles within the deposit for each of the CO contents. Unlike the particles within the oxide, the Ni content of these particles would be sufficient to catalyse C deposition [18, 19] and this is commensurate with their presence within the deposit. It is tempting, of course, to view the reducing Ni content of particles with increasing CO content as significant because this would provide a plausible physical mechanism for the effect of the CO content on deposit formation. It is a reasonable working hypothesis but some caution is required because of the inevitably limited number of particles that can be examined using TEM techniques. If the hypothesis is correct, the reduction in the Ni content of the particles could arise from an increased rate of gaseous nickel carbonyl formation in the higher CO gases but may also arise through a subtle change in the oxidation response of the alloy to the different environments that has yet to be identified.

An explanation for the partitioning of particle compositions between oxide and deposit is illustrated in Figure 10. It is envisaged that, during initial oxide formation, at Stage II, particles of a range of compositions are formed. It is proposed that those particles particularly rich in Ni catalyse the formation of filamentary C, become incorporated into the

filaments (e.g. Figure 1) and are removed from the sub-surface zone into the C deposits as the filaments grow. Those particles with lower Ni contents remain within the oxide. The differences in the size distributions shown in Figure 8, where fewer small particles were found within the oxide after exposures to the 0.7% CO gas compared with the 1.4% CO gas, may indicate that the smaller particles, of higher Ni content, are favoured catalytic sites and are removed into the deposit formed in the lower CO environment.

## 4. Conclusions

Carbon deposition on 20Cr25Ni steel at 700°C has been examined in $CO_2$-based gases containing 0.7%, 1.0% and 1.4% CO each with ~1000vpm $C_2H_4$. Filamentary carbon deposits were formed at the two lowest CO contents but not at 1.4% CO.

TEM characterisation has shown that, during the initial stages of oxidation in all three gases, Ni-rich metallic particles, also containing Fe, were formed within the surface oxide. Those, having mean diameters of 30-40 nm, catalysed C deposition in the 0.7 and 1.0% CO gases but not in that containing 1.4% CO.

Ni contents within the particles of approximately ≥75 at.% were required for catalytic behaviour and this value was not reached in the highest CO gas. In the 0.7 and 1.0% CO gases, it was found that particles with this high Ni content tended to be found within the carbon deposit whereas those with lower Ni contents remained within the oxide layer. A mechanism for this compositional partitioning is described.

## Acknowledgement

We are grateful to EDF Energy for their financial support of this work and to the staff at the Centre of Electron Microscopy at The University of Birmingham.

## Date availability

The raw data required to reproduce these findings cannot be shared due to technical limitations. The processed data required to reproduce these findings is contained within the paper.

## References


1. W.R. Martin and J.R. Weir, J. Nucl. Mater., **16**, (1965), 19-24.
2. R.A. Holm and H. E. Evans, Werkst. Korros., **38**, (1987), 166-175.
3. H.J. Grabke, Mater. Corros., **49**, (1998), 303-308.
4. T. Gheno, D. Monceau and D. Young, Corr. Sci., **64**, (2012), 222-233.
5. A. Fabas, A Rouaix-Vande Put, S. Doublet, D. Domergue, M Salem and D. Monceau, Corr. Sci. **123**, (2017), 310-318
6. A. Fabas, D. Monceau, C. Josse, P. Lamesle, A R-V Put, Corr. Sci., **107**, (2016), 204-210.
7. D.J. Young, J. Zhang, C. Geers, M. Schütze., Materials and Corrosion. 2011;62 (1),7-28.
8. G.R. Millward, H.E. Evans, M. Aindow and C.W. Mowforth, Oxid. Metals, **56**, (2001), 231-250.
9. R.T.K. Baker, M.A. Barber, P.S. Harris, F.S. Feates and R.J. Waite, J. Catal., **26**, (1972), 51-62.
10. R.A. Holm and H.E. Evans, Werkst. Korros., **38**, (1987), 219-224.
11. R.A. Holm and H.E. Evans, Werkst. Korros., **38**, **(**1987), 224-229.
12. H.J. Grabke, E.M. Müller-Lorenz, B. Eltester and M. Lucas, Mater. High Temp., **17**, (2000), 339-345.
13. M. Hänsel, C.A Boddington and D.J. Young, Corros. Sci., **45**, (2003), 967-981.
14. J. Zhang, K. Boddington and D.J. Young, Corros. Sci., **50**, (2008), 3107-3115.
15. E. Flahaut , A. Govindaraj, A. Peigney, Ch. Laurent, A. Rousset and C.N.R. Rao, Chemical Physics Letters 300, (1999), 236–242
16. M. Taylor, H. Evans, P. Smith, R. Ding, Y-L. Chiu, S Rai, B. Connolly, N. Smith, L. Pearson, C. Mowforth. Oxid Met., **87,** (2017):667–678
17. Handbook of Chemistry and Physics, 65$^{th}$ Edition, Robert C. Weast, Editor in Chief, CRC Press, (1984).
18. C. Park and R. T. K. Baker, J. Catal., **190,** (2000), 104-117.
19. C. Park and R. T. K. Baker, J. Catal., **179,** (1998), 361-374.

Table1. Compositions (at.%) of the oxide scale of samples tested in each gas.

| CO content of gas, vol.% | O | Cr | Fe | Ni | Mn | Cr/Fe |
|---|---|---|---|---|---|---|
| 0.7 | 65.2 ± 1.4 | 25.1±1.2 | 9.2±1.0 | 0.04±0.04 | 0.47±0.38 | 2.76 ± 0.4 |
| 1.0 | 64.3 ± 1.5 | 25.2±2.3 | 9.5±1.1 | 0.13±0.06 | 0.84±0.17 | 2.70 ± 0.6 |
| 1.4 | 67.4 ± 1.3 | 23.2±1.5 | 8.8±1.9 | 0.3±0.5 | 0.24±0.29 | 2.80 ± 0.9 |

Table 2. Size and number density of particles within the oxide of samples exposed to gases of different CO contents.

| CO content of gas, vol.% | Mean equivalent diameter, nm | Number density per unit volume, $m^{-3}$ |
|---|---|---|
| 0.7 | 39 ± 8 | $2.68 \times 10^{21}$ |
| 1.4 | 34 ± 7 | $2.86 \times 10^{21}$ |

Table 3. Compositions of the particles within the oxide of samples tested in each gas.

| CO content of gas, vol.% | Ni/Fe ratio | Mean Ni content, at.% |
|---|---|---|
| 0.7 | 2.54 ± 0.20 | 71.8 ± 2.7 |
| 1.0 | 2.26 ± 0.66 | 69.3 ± 3.0 |
| 1.4 | 2.48 ± 0.36 | 71.3 ± 2.5 |

Table 4. Compositions of the particles within the C deposit for samples exposed to 0.7 and 1.0% CO containing gas.

| CO content of gas, vol.% | Ni/Fe ratio | Mean Ni content, at.% |
|---|---|---|
| 0.7 | 7.9 ± 4.5 | 88.8 ± 2.8 |
| 1.0 | 3.9 ± 0.9 | 79.6 ± 3.0 |

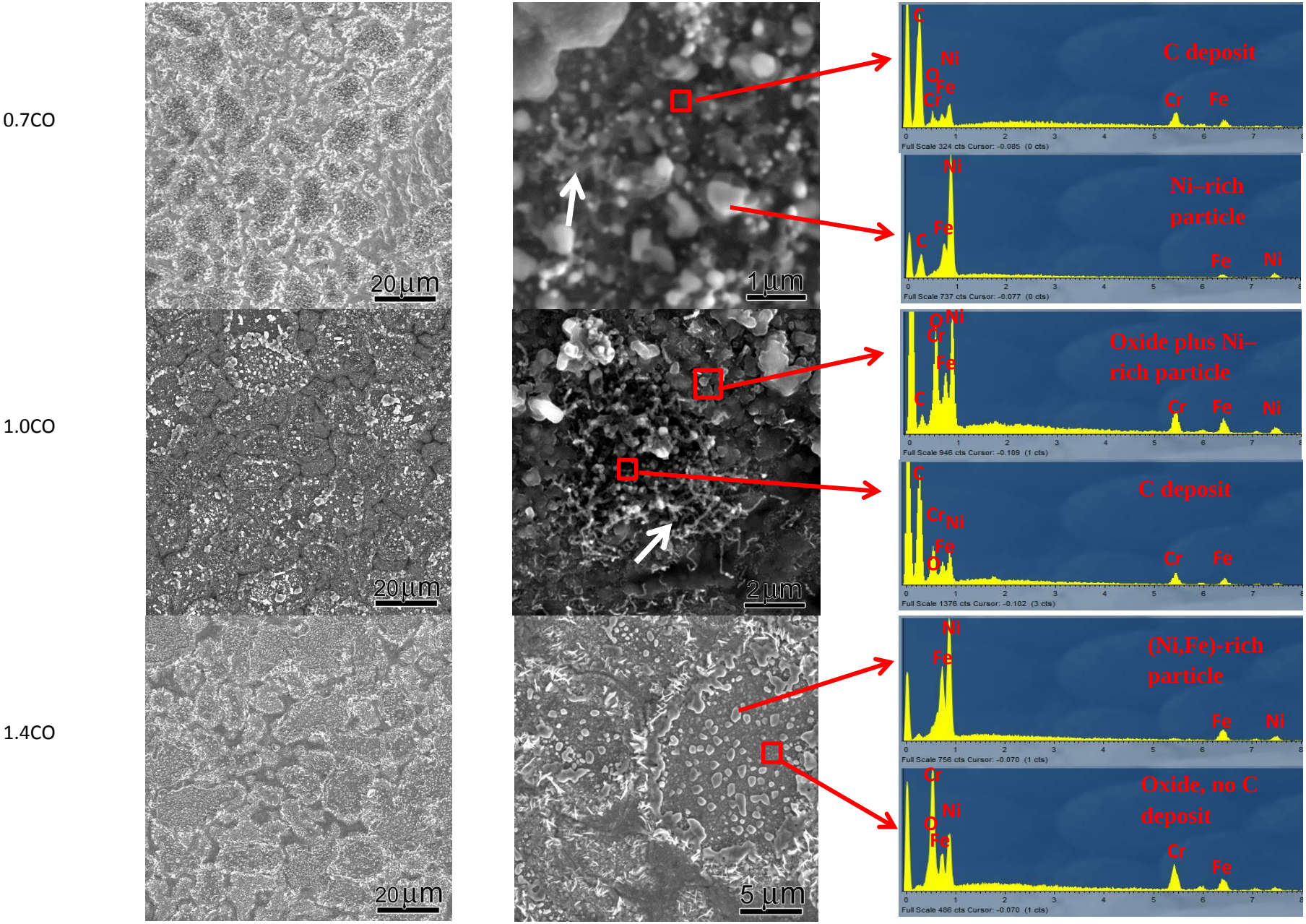


Figure 1. SEM images and EDS spectra of the surfaces of the samples, after exposure to 0.7%, 1.0% and 1.4% CO at 700°C for 4 hours. Note: filarmentary carbon deposits were observed in the regions indicated by white arrows.

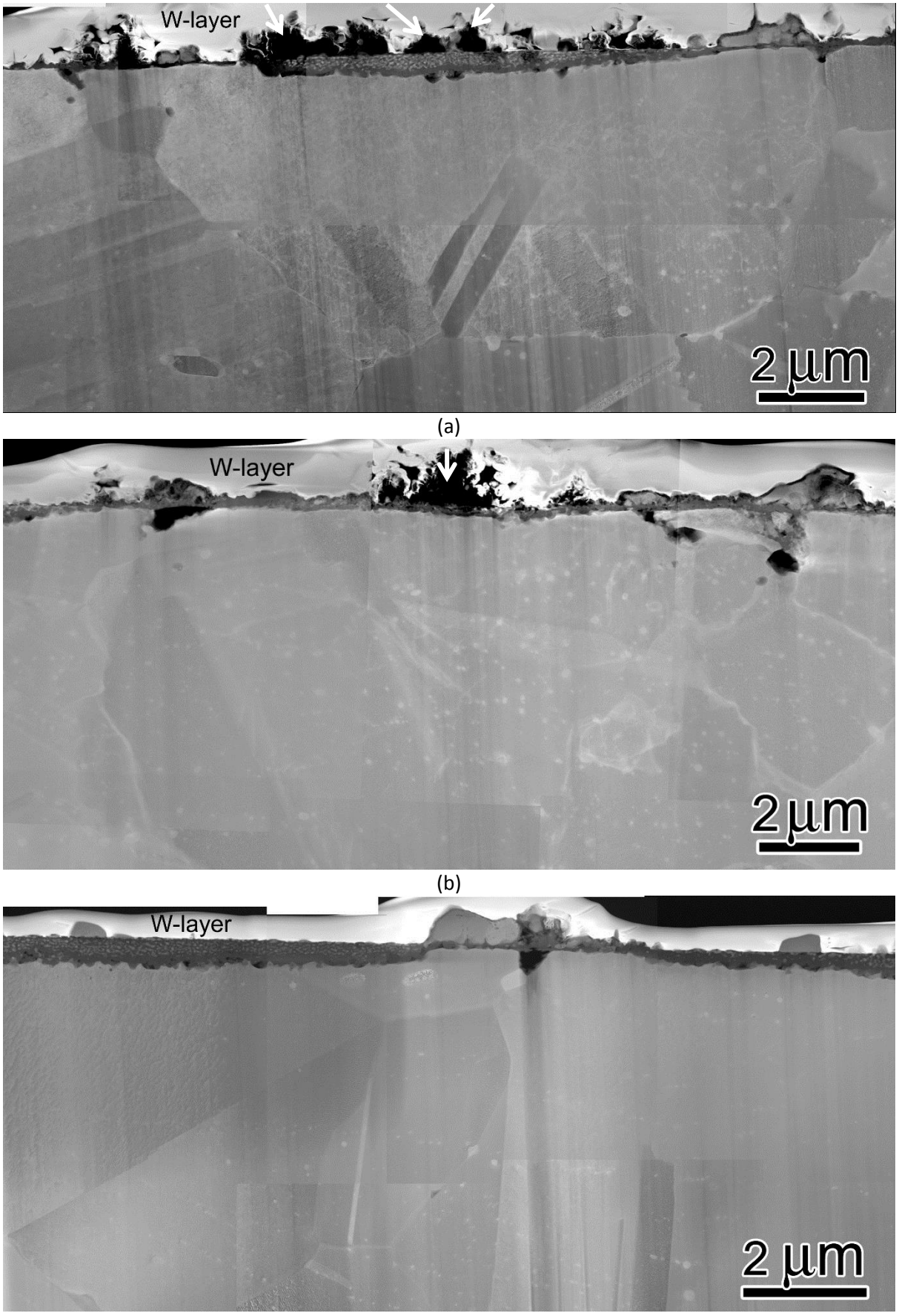


Figure 2. STEM images of the surfaces of the samples after exposure to the (a) 0.7%, (b) 1.0% and (c) 1.4% CO containing gases, at 700°C for 4 hours. C deposits (arrowed in Figs 2a and 2b) were observed on the samples exposed to 0.7% and 1.0%CO.

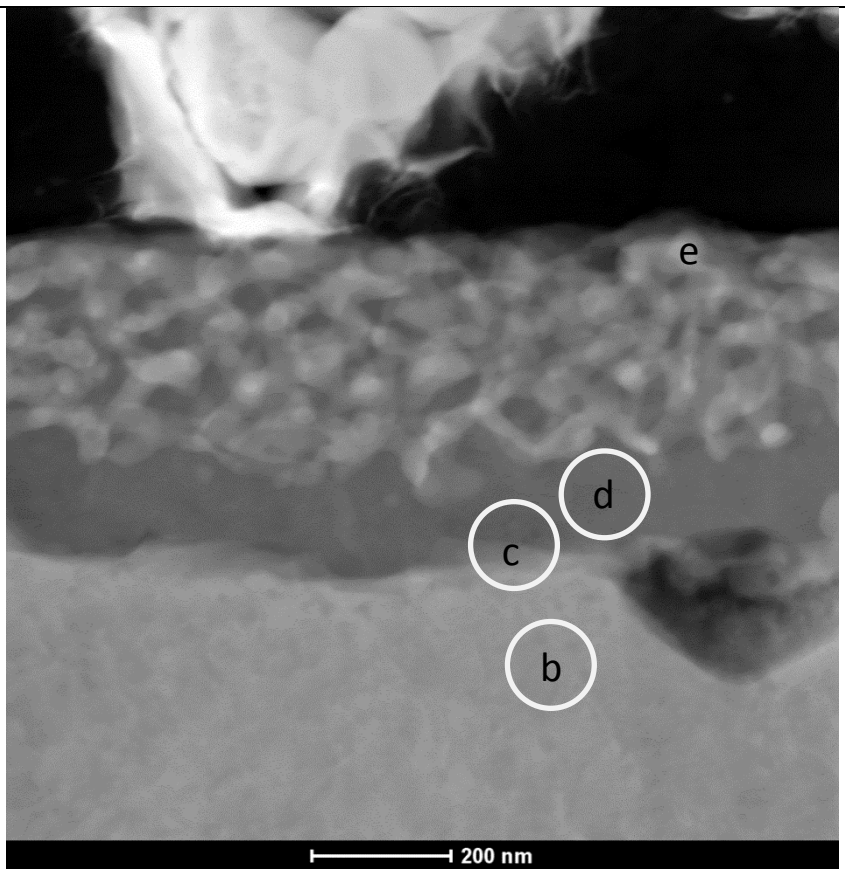


(a)

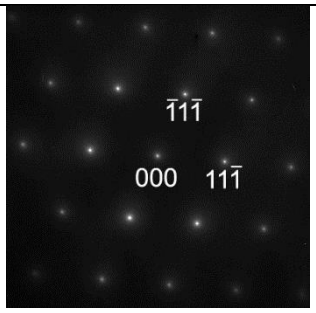


(b) [011] alloy from A

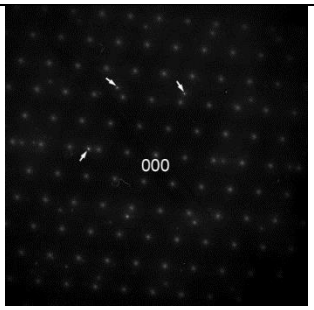


(c) oxide+alloy from B

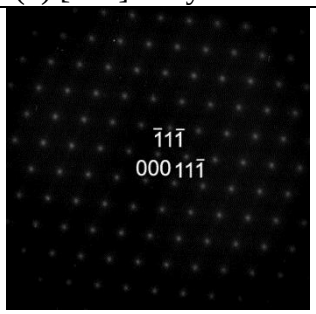


(d) [011] oxide from C

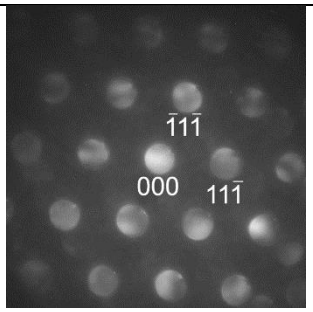


(e) [011] CBED of the particle as shown in D

Figure 3. (a) STEM-HAADF image through the surface region of the sample exposed to 0.7% CO-bearing gas with electron patterns taken for: (b) the alloy, (c) the alloy and oxide, (d) oxide and (e) the nickel-rich particle. This shows that the nickel-rich feature in (e) has the same crystal orientation and FCC structure as the alloy in (b) and that the oxide is identified as spinel phase (FCC structure - $(Cr,Fe)_3O_4$ with lattice parameter a =0.84 nm. Note: the spots (arrowed) in Fig. 3c are from the alloy.

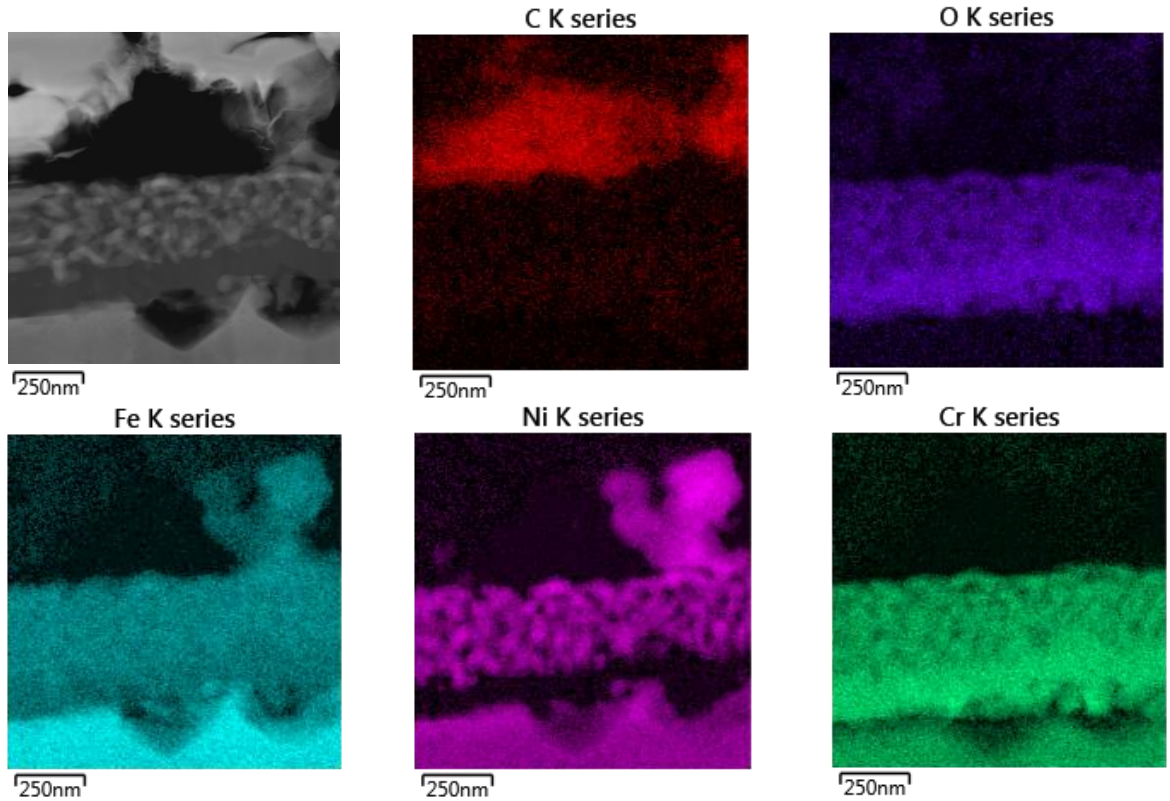


Figure 4. EDS maps from the C deposit and the oxide in the sample exposed to the 0.7%CO gas, showing that C deposited on the oxide surface, that the particles in the C deposit and at the upper part of the oxide layer are rich in Ni, and that the oxide is Cr-rich.

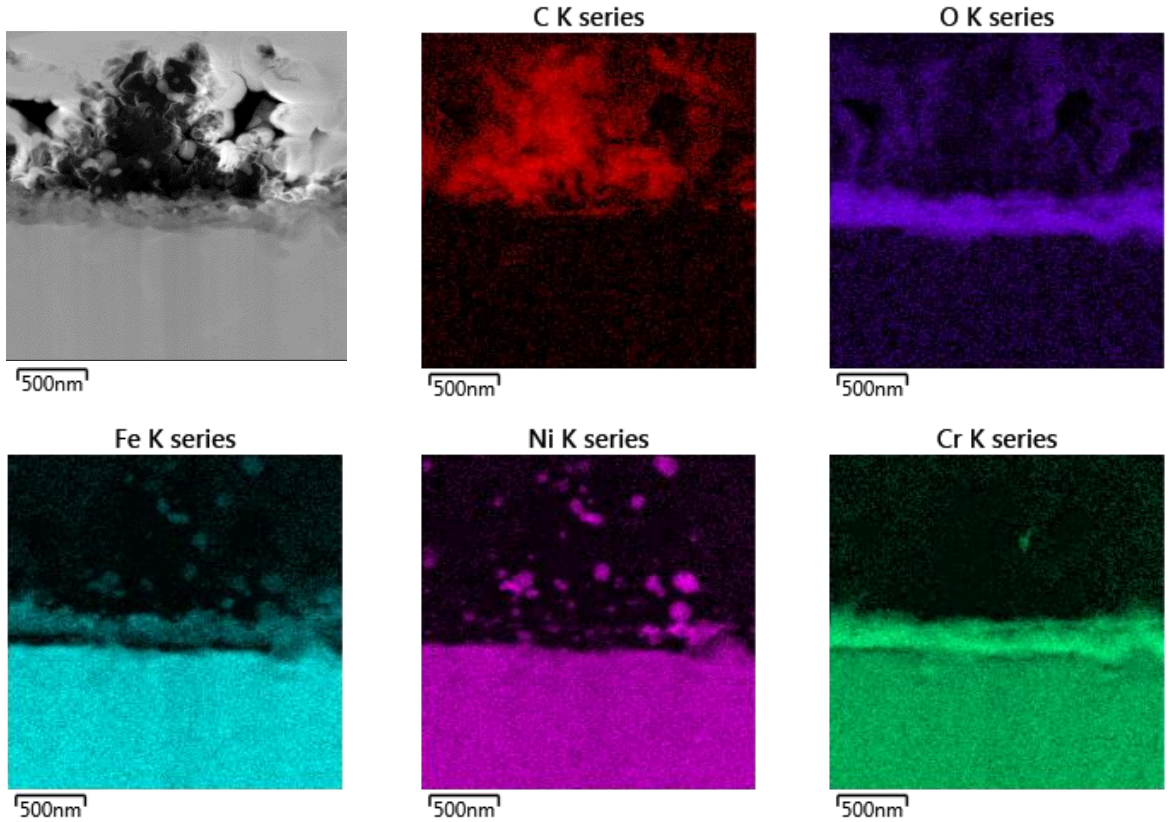


Figure 5. EDS maps from the C deposit and the oxide in the sample exposed to the 1.0%CO gas, showing that C deposited on the oxide surface and that the particles in the C deposit and at the upper part of the oxide layer are rich in Ni.

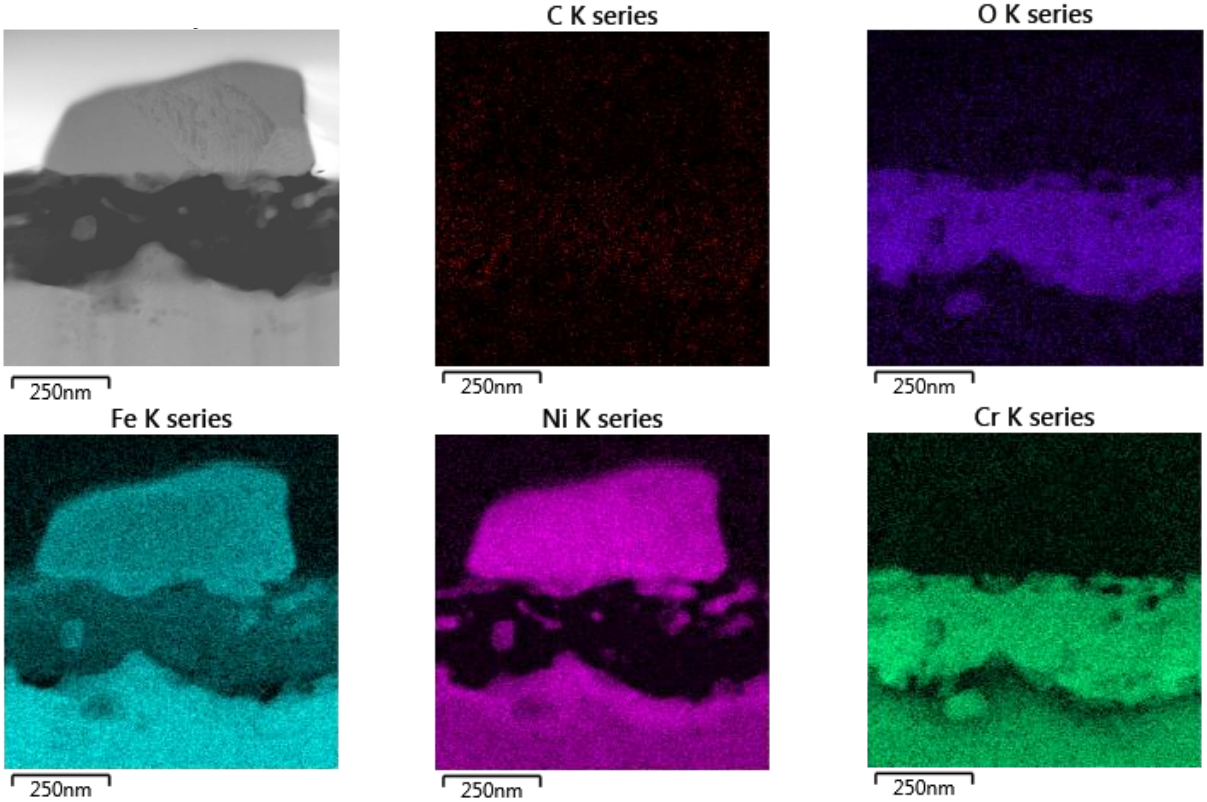


Figure 6. EDS maps from the oxide in the sample exposed to the 1.4%CO gas, showing that the top big particle is rich in Fe and Ni and that the particles within the oxide are rich in Ni and Fe. Note: no C deposit was formed in this gas composition. The maps for the minor elements (Mn, Nb) resulted in background level readings only and are omitted from this figure.

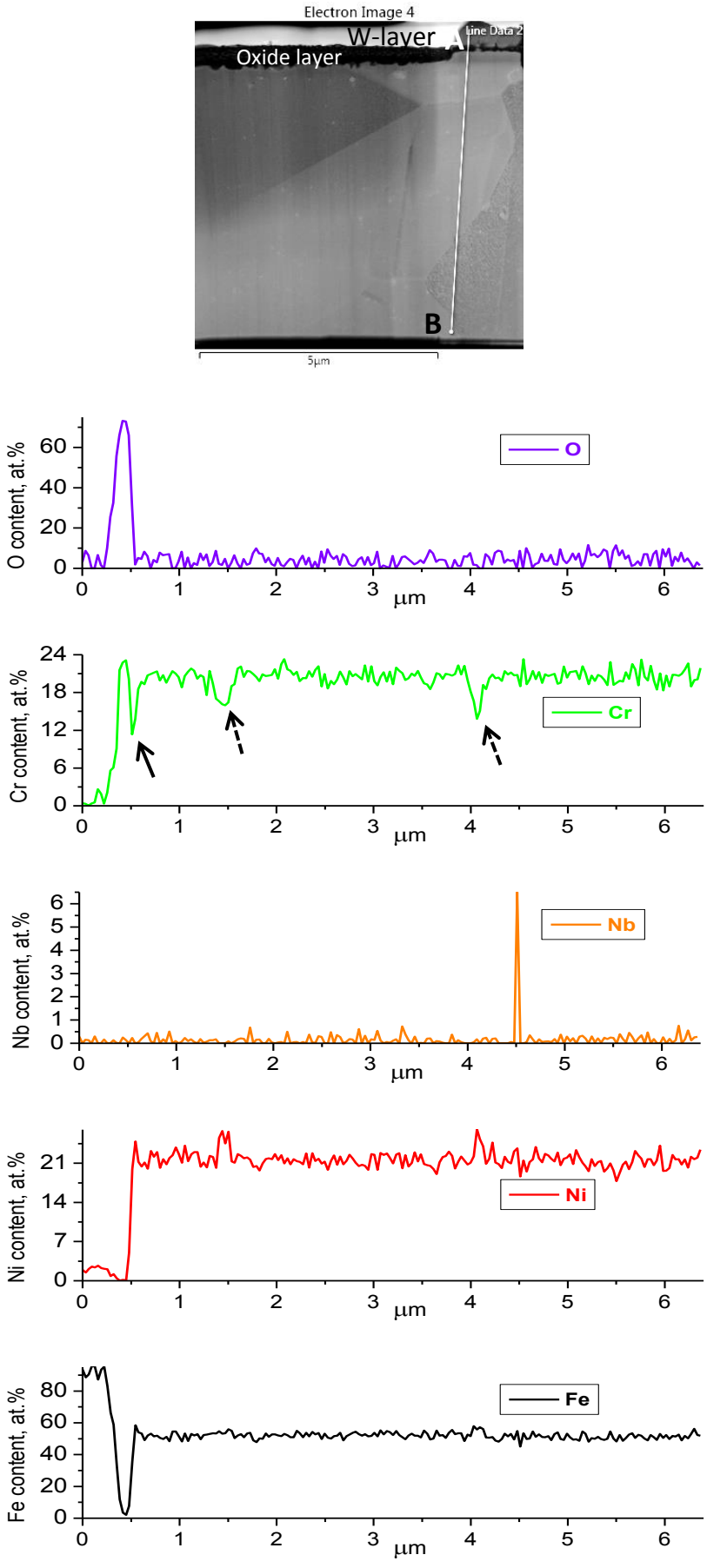


Figure 7. EDS linescan (from A to B in the electron image) from oxide into the alloy including grain boundaries for the sample after exposure to 1.4%CO, showing a ~100 nm Cr

depleted region (solid black arrow) underneath the surface oxide and grain boundary Cr depletion (dashed arrows at 1.5 and 4.0 μm). Note: the Nb peak is probably associated with Nb carbide.

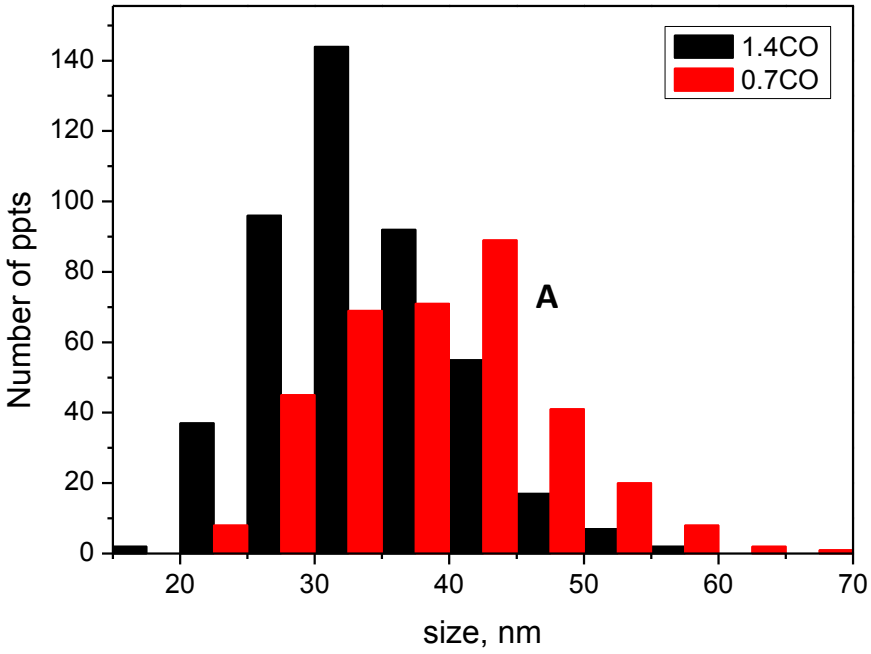


Figure 8. The size distribution of Ni-rich particles within the oxide layer in the samples, after exposure to 0.7 % and 1.4 %CO.

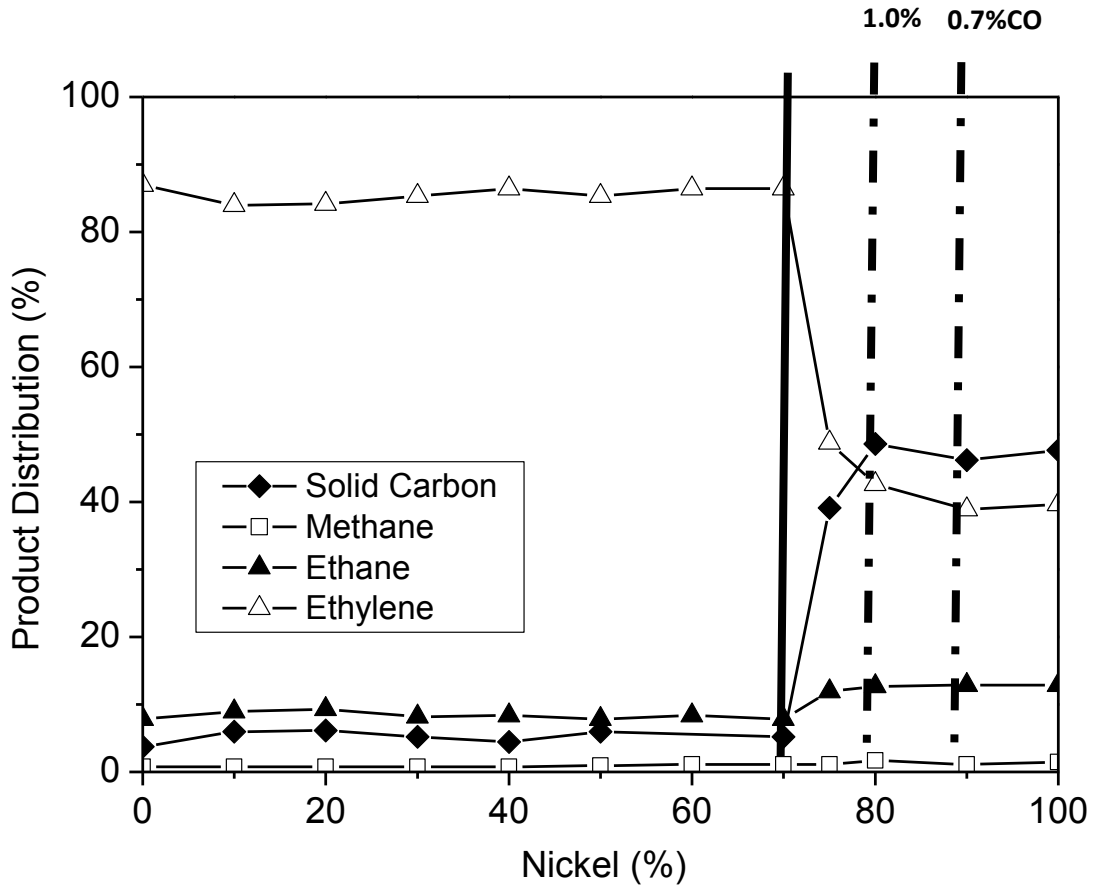


Figure 9. The percentage product distribution from the hydrogenation of a $C_2H_4/H_2$ (4:1) mixture over various Fe-Ni powders at 600$^{o}$C [19]. The solid vertical line corresponds to the Ni content of particles within the oxide, in the present work, for all CO concentrations. The two dashed lines give the Ni contents of particles within the deposit for the 0.7 and 1.0% CO gases as indicated on the figure.

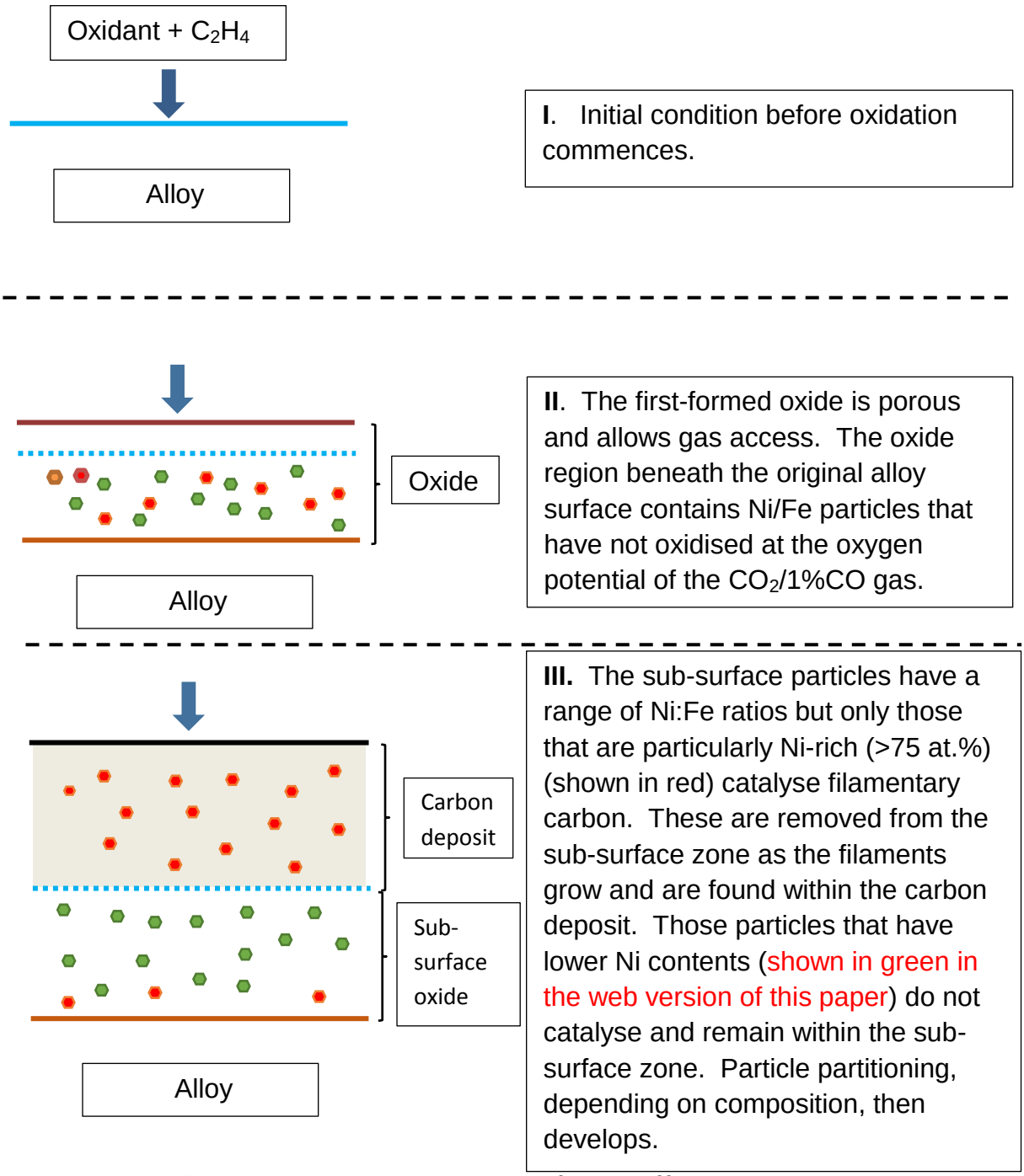


Figure 10. Schematic diagram proposing an explanation for the difference in the composition of the particles found at the two sites, i.e. within the oxide and within carbon deposits.